PPPL-2150

PPPL-2150

UC20-F

DE-0574-6

I-17987

ELECTRON TEMPERATURE MEASUREMENTS DURING ELECTRON CYCLOTRON HEATING ON PDX USING A TEN CHANNEL GRATING POLYCHROMATOR

By

A. Cavallo, H. Hsuan, D. Boyd, B. Grek, D. Johnson, A. Kritz, D. Mikkelsen, B. LeBlanc, H. Takahashi

OCTOBER 1984

PLASMA PHYSICS LABORATORY

PRINCETON UNIVERSITY
PRINCETON, NEW JERSEY

PREPARED FOR THE U.S. DEPARTMENT OF ENERGY, UNDER CONTRACT DE-AC02-76-CHO-3073.

ELECTRON TEMPERATURE MEASUREMENTS DURING ELECTRON CYCLOTRON HEATING ON PDX USING A TEN CHANNEL GRATING POLYCHROMATOR

A. Cavallo, H. Hsuan,

D. Boyd+, B. Grek, D. Johnson,

A. Kritz++, D. Mikkelsen, B. LeBlanc,

H. Takahashi

Princeton Plasma Physics Laboratory, Princeton, N.J.

+U. of Maryland, College Park, Md.

++Hunter College/CCNY, N.Y.

PPPL--2150

DE85 002701

ABSTRACT

During first harmonic electron cyclotron heating (ECH) on the Princeton Divertor Experiment (PDX) (R_o = 137 cm, a = 40 cm), electron temperature was monitored using a grating polychromator which measured second harmonic electron cyclotron emission from the low field side of the tokamak. Interference from the high power heating pulse on the broadband detectors in the grating instrument was eliminated by using a waveguide filter in the transmission line which brought the emission signal to the grating instrument.

Off-axis (~ 4 cm) location of the resonance zone resulted in heating without sawtooth or m = 1 activity. However, heating with the resonance zone at the plasma center caused very large amplitude sawteeth accompanied by strong m = 1 activity: $\Delta T/T_{MAX}$ = 0.41, sawtooth period ≈ 4 msec ,m = 1 period ≈ 90 μ sec, (11 kHz). This is the first time such intense MHD activity driven by ECH has been observed. (For both cases there was no sawtooth activity in the ohmic phase of the discharge before ECH.) At very low densities there is a clear indication that a superthermal electron population is created during ECH.

1. INTRODUCTION

From fundamental plasma physics considerations, plasma heating in a tokamak at the electron cyclotron frequency is very attractive. The wave-plasma interaction has been studied extensively both theoretically and experimentally and is well understood.[1] This interaction is expected to be independent of plasma edge conditions and impurity content. The power deposition is localized and the position of the heating zone can be easily controlled. Finally, the antenna-plasma coupling problem is neatly and easily solved. With the further development of the gyrotron,[2] the lack of a reliable, efficient high power source is being overcome.

Two 60-GHz, 200-kW Varian gyrotrons (100-msec maximum pulse length) were available for heating experiments on PDX. Power was launched from the low field side of the tokamak in the O-mode (wave E-field parallel to toroidal B field); a reflector mounted opposite to the launcher converted the incident O-mode to a reflected X-mode (wave E field perpendicular to toroidal B field). An antenna was also available on the high field side for current drive and heating. However, for the experiments to be described only the outer antenna (O-mode) and a single gyrotron were used.

A unique feature of the PDX ECH system was the attention paid to the design of the transmission line and antenna.[3,4] Power from the gyrotron in the TE02 mode was converted to a low loss TE01 mode for transmission to the tokamak, which was located 30 meters from the gyrotron. At the tokamak, the TE01 mode was converted first to a TM11 mode, then to an HE11 mode for launch from an open waveguide. This mode has a gaussian antenna pattern with 10 dB points (full width) of 10 cm at the plasma center. This narrow antenna pattern ensured that power deposition was very well localized, which was essential for this experiment.

2. INSTRUMENTATION

A. General Principles

Electron temperature evolution was determined using a ten channel grating polychromator[5] which measured second harmonic X-mode emission from the plasma. For the plasma conditions of interest this was black body emission, that is, the emission intensity depends only on local temperature, not local density or impurity content. The electron cyclotron frequency is determined by the local toroidal magnetic field, given by $B_T = B_o R_o / R$. Here B_o is the toroidal field at a major radius R_o, and R is an arbitrary major radius. Thus, a measure of the emission intensity at a known frequency yields electron temperature at a corresponding position in the plasma.

In the grating instrument (Fig. 1) the entrance aperture and mirror M1 serve to illuminate the grating with a plane wave; lens L1 acts to correct the aberration introduceed by using M1 45° off axis. The grating then disperses the light according to the relation:

$$2d \sin(\sigma + S_n) \cos S_n = K\lambda_n \quad (K = 1, 2\ldots;\ n = 1\ldots10). \qquad (1)$$

Here d is the grating constant, σ is the angle between the incident beam and the grating normal, $2S_n$ is the angle between the incident beam and the output beam from the grating which is focused by mirror M2 on the n^{th} exit aperture, and K is the order of the interference.

The light is detected by liquid helium cooled indium antimonide hot electron bolometers[6] housed in a long hold cryostat. The detector rise time is less than 1 μsec (200 kHz 3 dB point), that of the detector preamplifier, 7 μsec (25 kHz 3 dB point), and the minimum detectable signal between 10 and 40 eV RMS (best and worst detectors) with a 9 kHz 3 dB point.

B. Waveguides and Antenna

The light transport system for the PDX experiment is shown in Fig. 2. C-Band waveguide (47.5 mm x 22.15 mm) was used except for a 200 cm C-Band to F-Band to C-Band waveguide filter. Six 90° bends (4E plane and 2H plane) were used and the total length of the waveguide run was about 15 meters. The theoretical loss (waveguide and bends) for single mode transmission was about 3 dB at 120 GHz for this system.

Spatial resolution is determined by two factors. Resolution along the major radius is set by the frequency resolution of the grating instrument, and is about 3 cm (3 dB point). The spot size of the waveguide stub antenna viewing the plasma determines vertical and horizontal resolution. For the single mode system used in this experiment the vertical resolution was about 6 cm, and the horizontal resolution about 13 cm (10 dB points) at R = 140 cm as calculated from Ref. 7. Antenna spot size could have been reduced by moving a smaller waveguide stub closer to the plasma, but this would have blinded another diagnostic.

C. Filters

A major problem with electron cyclotron emission measurements during this experiment was that the broadband detectors, which must detect a few tens of nanowatts at 120 GHz, are sensitive to stray radiation from the 60-GHz, 100-kW heating pulse. Such interference was completely eliminated by inserting a waveguide filter with a cutoff at 73.76 GHz (F Band) into the transmission line. The linear tapers used (C Band to F Band to C Band) had a theoretical loss (mode conversion) of about 10% each.

Instrument sensitivity with the filter in place was reduced by a factor of 3.5 to 5.5. Although this was a severe penalty, a signal to noise ratio greater than 100:1 (RMS) for five of the ten channels, was still obtained and was adequate for these measurements.

The magnitude of the reduction in sensitivity was somewhat larger than expected, as can be seen from the following analysis. The polarizer near the input to the transmission line (Fig. 2) allows only TE_{NO} modes (N = 1,2,3...) to propagate in the waveguide. However, diffraction at the input aperture of the grating instrument (50 mm x 12 mm, wave E field parallel to the short dimension of the aperture) is such that only the first two TE modes are well coupled to the input mirror. Since, for black body emission, energy per waveguide mode is $kT_e\Delta f$, where k is Boltzmann's constant, T_e is the electron temperature, and Δf the frequency resolution (~ 2.4 GHz) of the instrument, this diffraction limits the energy throughput of the grating polychromator.

Thus, insertion of a waveguide filter which allows only a single TE mode to pass should reduce the throughput by about a factor of two, not including resistive losses in the linear tapers and the fundamental waveguide, which should be of the order of 1 dB.

The only other factor which could account for the higher than expected attenuation is the misalignment of the transmission line. This would convert energy in the fundamental mode to higher modes which would be rejected by the mode filter.

One further problem with a grating instrument can be seen from Eq. (1). A channel tuned to accept power at a wavelength λ also accepts power at $\lambda/2$, $\lambda/3$, etc., i.e., at higher orders. Low pass grating filters[8] were mounted in the 90° waveguide bends. These had a very rapid rolloff (100 dB/octave), low attenuation in the passband and eliminated higher order light from the input to the instrument.

D. Calibration

The system was calibrated by normalizing the output of each of the ten channels to the electron temperature measured at the corresponding channel radius by T.V. Thomson Scattering (TVTS) on several ohmic discharges. The error bars shown on Figs. 5, 6, and 8 on the T_e profiles using ECE data reflect the uncertainty in the calibration constant of each channel. The uncertainty arises from discharge to discharge irreproducibility of the plasma and system noise present in both the ECE and TVTS data; both systems measure a profile along a major radius in the equatorial plane.

It is important to note that the ECE system averages the electron temperature over a much larger plasma volume (3 cm x 6 cm x 13 cm) than does TVTS (1 cm x 1 cm x 1 cm). Poor resolution along the toroidal field (13 cm resolution - 10 dB point) is not important since temperature gradients in this direction are negligible. However, the poorer radial and vertical resolution can lead to lower electron temperatures at the plasma center, compared to Thomson scattering data, especially during sawtooth activity. Fortunately, in this case, the volume of plasma involved is small, so that this deficiency is tolerable.

3. ELECTRON CYCLOTRON HEATING (ECH) RESULTS

A. On-axis Location of the Resonance Zones

Electron heating with the resonance zone located close to the center of the plasma is shown in Fig. 3. The central electron temperature rose rapidly (e-folding time ~ 7 msec), and strong sawtoothing (period ~4 msec) began about 10 msec after the start of the heating pulse. That the $T_e(o)$ rise time is much shorter than the heating pulse indicates that, at least for understanding the gross features of plasma behavior during ECH, a 40-msec pulse is adequate.

When the heating pulse ended, the central T_e fall time was much greater than the initial rise time. For example, in Fig. 3, T_e (R = 144.4 cm) remains nearly constant for about 50 msec after the end of the heating pulse. The post-heating behavior of the electron temperature will be discussed in a later section.

An expanded view of the sawteeth generated during ECH is shown in Fig. 4. The distortion in the temperature rise during ECH on these signals is caused by the 8-Hz low-frequency 3 dB point of the digitizer preamplifier. The sawtooth period is around 4 msec, but is in fact somewhat irregular(± 0.5 ms), perhaps due to the presence of a large amplitude m = 1 oscillation with a frequency of about 11 kHz. (Strictly speaking, one can only say from Fig. 4 that this is an m-odd oscillation, but since it is so closely associated with the termination of the sawtooth, it is reasonable to label it as m = 1.) This oscillation continues for about one-half the sawtooth period, in contrast to what is observed during an ohmic heating sawtooth, where the m = 1 only appears immediately before the disruption; frequently only one or one-half cycle of the m = 1 is seen in ohmic sawtooth.

The 180° change in phase on the m = 1 oscillation between R = 133 cm and R = 139 cm indicates that the center of the discharge is near R = 136 cm, and that the maximum T_e was not observed by the grating instrument.

A comparison between ECE and TVTS data is shown in Fig. 5 (top of a sawtooth) and Fig. 6 (700 μsec after sawtooth collapse). These are two similar discharges; note that the maximum central T_e is observed by TVTS at the top of a sawtooth, and that the ECE data points straddle the peak of the T_e profile and are in excellent agreement with TVTS. The amplitude of the T_e sawtooth is far larger than what is normally observed during ohmic, ICRH, or beam-heated discharges. Here it is found that $\Delta T/T_{MAX} \simeq 0.41$, and that the central T_e drops by about 900 eV from 2.45 keV to 1.55 keV in less than 50 μsec in a typical internal disruption.

It is clear that, because of the presence of such large sawteeth, the figure of merit usually employed to characterize tokamak heating must be applied with discretion. This figure of merit is defined as the measured central temperature increase (ΔT) times the average density ($\bar{N}_e$) divided by the RF input power (P_{RF}). For the case of ECH with the resonance zone located at the center of the plasma, the figure of merit is ($\bar{N}_e = 0.6 \times 10^{13}$ cm^{-3}, P_{RF} = 75 kW):

top of sawtooth:	9.2×10^{13} eV/kW cm^3
bottom of sawtooth:	2×10^{13} eV/kW cm^3
average (middle of sawtooth):	5.6×10^{13} eV/kW cm^3

B. Off-axis Location of the Resonance Zone

The time evolution of the electron temperature during ECH (R_{RES} =141.7 cm, R_o = 135 cm) is shown in Fig. 7. In this case, a rapid rise (e-folding time ~ 7 msec) was followed by a gradual increase in central T_e but without the generation of any MHD activity. The fall time in $T_e(o)$ after the heating pulse was, as for the case of on-axis heating, much greater than the rise time.

The figure of merit for off-axis heating is ~ 5.5×10^{13} eV/kW-cm^3 ($\bar{N}_e$ = 10^{13} cm^{-3}, P_{RF} = 80 kW). This compares very favorably with what is observed [9] with neutral beam heating and ICRH on PLT, 2.5-4×10^{13} eV/kW-cm^3.

A comparison between the TVTS temperature profile and the ECE profile is shown in Fig. 8 for off-axis heating. Once again, the good agreement between the two diagnostics indicates that bulk heating is obtained and production of nonthermal electrons is very small.

C. Post Heating Changes in the Electron Temperature Profile

The slow decay of the central electron temperature after on-axis or off-axis heating (Figs. 3 and 7) remains difficult to explain. At first it seemed as if the rapid rise in line average density after ECH - 50% in 150 msec (Fig. 9) - might cause this slow decay. In another experiment in which line average density was better controlled, this density rise and the slow T_e decay were absent. However, results from a computer simulation (Section 4 and Fig. 12) indicate that this density rise cannot cause such an effect. Thus, this point remains unclear and hopefully will be investigated in a future series of experiments.

D. ECH in Very Low Density Regime

It is well known that ECH power in the X-mode, first harmonic, incident from the high field side of the tokamak can preferentially increase the perpendicular energy of the high energy tail of the electron distribution.[10] In the very low density regime ($\bar{N} \approx 0.13 \times 10^{13}$ cm^{-3}), (Fig. 10) the optical depth at the first harmonic O-mode is: $\tau_{0,1} \simeq 0.2$ (T_e = 2 keV). Almost 80% of the incident O-mode power is available to be converted to X-mode in a poorly focused beam for additional heating (Power Transmitted/Power Incident = $e^{-\tau}$). This situation is ideal for the production of nonthermal and runaway electrons.

From Fig. 10 it can be seen that the emission from the outer portion of the plasma increased much more than the emission from the center of the plasma during heating. After the heating pulse, emission from the central and outer regions at first decayed, but then increased rapidly as the discharge ran away.

Because the optical depth of the outer portion of the plasma is less than that of the center, emission from this region is more sensitive to the presence of nonthermal electrons in the discharge. Thus, the large relative increase in emission during heating measured by the channel labeled R = 155 cm is a clear indication of the buildup of the superthermal population.

In fact, for this low density discharge, ξ, the ratio of the mean drift velocity to the random thermal velocity, is of order one even before the start of the heating. It is, therefore, difficult to distinguish between the importance of the ohmic heating electric field and the ECH in creating runaways. However, the fact that runaway only occurs 20 milliseconds after the heating indicates that the interaction between the superthermal population and the ohmic electric field is not the dominant one during ECH.

An estimate of $T_\perp(0)$ of the superthermal population created during ECH can be made for this discharge. Since the resonance zone is located at the plasma center (R = 136 cm), the superthermal population should be localized in this region. The emission observed on the channel labeled R = 155 cm (f = 104.3 GHz) for thermal electrons actually originates at the plasma center: because of the relativistic mass increase of the superthermal electrons, their emission frequency is downshifted from f = 118.8 GHz (R = 136 cm) to f = 104.3 GHz. The relativistic mass increase is given by m_o[f(136 cm)/f(155 cm)], where M_o is the rest mass of the electron. This indicates that $T_\perp(0) \lesssim$ 70 keV. The equipartition time for such electrons with the background plasma [$T_e(0) \approx 2$ keV, $N_e(0) \approx 1.8 \times 10^{-2}$ cm^{-3}, $Z_{eff} \approx 2$] is approximately 22 msec. Thus, these energetic electrons are decoupled from the bulk electron distribution.

A more sensitive test for the creation of superthermal electrons during electron cyclotron heating is the simultaneous measurement of second harmonic emission on the high- and low-field side of a tokamak[11] in a discharge where ξ is much less than 1. In the present experiment, one has a clear indication that ECH can indeed create a superthermal population and modify the electron velocity distribution substantially, but a more thorough study remains to be done.

4. RESULTS FROM THE COMPUTER SIMULATION

Since the power deposition profile during electron cyclotron heating is understood, it is possible to study electron energy transport using ECH. This is of fundamental importance, as the major energy loss channel in a tokamak plasma is via anomalous electron heat conductivity. Global electron energy transport is much larger than what is predicted by neoclassical theory, even though ion energy transport is of the same order as that given by this theory.

To investigate transport, BALDUR,[12] a one-dimensional transport code, has been coupled to a ray tracing code which computes ray paths and associated power deposition in the plasma. The line average density and the loop voltage and current are used as inputs in the BALDUR code. The transport coefficients are modelled such that the simulation temperature and density profiles are consistent with the TVTS profiles obtained during an ohmic discharge. The location of the plasma center was determined from an MHD equilibrium solution to the Grad-Shafranov equation.

The transport model used for the BALDUR ECH simulation is summarized in Table II. Other assumptions are that impurity radiation for these low density diverted discharges is negligible, and that the density is controlled by adjusting a gas puffing rate to produce the desired line average density.

Results of the simulation for the case of off-axis heating ($r = 4$ cm) are shown in Fig. 11. Good agreement is obtained between the simulation and TVTS and second harmonic ECE measurements with a single transport model used in both the OH and ECH phases. In addition, the same χ_e (electron thermal conductivity) model which fits the data with the resonance located off-axis also fits the data for the on-axis heating case.

The observed evolution of $T_e(0)$ for the case of on-axis heating is compared to that calculated by the computer simulation in Fig. 12. Note that the simulation predicts a rapid drop in the central temperature after heating, which is very different from what is observed in the experiment (Figs. 3 and 7). The time evolution of $\bar{N}_e$ (line average density) used in the simulation is shown in the insert in Fig. 12A. Therefore, the slow $T_e(0)$ decay after ECH cannot be explained by the use in line average density after ECH.

Experimental data for a case of on-axis heating in which $\bar{N}_e$ was better controlled is shown in Fig. 12B. Here $\bar{N}_e$ decreased during heating but then only rose to its preheating value (insert, Fig. 12B). This discharge was identical to the one previously studied except for the post heating behavior of the line average density. In this case, simulation and experiment are in much better agreement with respect to the post heating behavior of the central electron temperature. Yet the reason for this remains unclear. It is hoped this can be resolved in a future experiment.

In these experiments, the auxiliary heating power ($\leq$ 80 kW) was much less than the total ohmic heating power (~ 250 kW). However, locally the ECH power was equal to or greater than ohmic heating power for a plasma radius $r \approx \leq 20$ cm. Therefore, that the results can be matched with a transport model which does not change during heating is very encouraging but not unexpected, since the discharge is not really changed very much globally. Still, substantial changes could be made in the discharge with the resonance zone located near its center; profile control was clearly demonstrated in these experiments. These experiments will have to be repeated at power levels of the order of the ohmic heating power before any definitive conclusions about global transport can be drawn.

5. CENTRAL POWER DEPOSITION

Ray tracing calculations indicate that almost all of the ECH power is deposited inside the sawtooth inversion radius. These calculations can be checked roughly by using the measured rate of rise of $T_e(0)$ during a sawtooth as follows

$$P_D = \frac{dT_e(0)}{dt} \cdot N_e(0) \cdot \frac{3}{2} \cdot 2\pi^2 R_o b^2 \cdot a \ .$$

Here P_D is deposited power from ohmic heating as well as electron cyclotron heating, a is a constant which depends on the shape of the T_e profile inside the inversion radius b, R_o is the plasma major radius, and $N_e(0)$ is the electron density inside the inversion radius. For the peaked profiles obtained from on-axis heating, we have taken a = 0.5 (triangular profile). From other grating instrument T_e measurements, the inversion radius for the sawtooth is located at R = 145 ± 1 cm; b = 8 cm. With R_o = 137 cm and $dT_e(0)/dt$ = 900 eV/4 x 10^{-3}sec, we have P_D = 70 kW. This is in quite reasonable agreement with calculations which indicate that about 80 kW total heating power is deposited inside the inversion radius for on-axis heating.

6. DISCUSSION

It is evident that the grating instrument is able to follow electron temperature profile evolution during electron cyclotron heating experiments. Interference from the high power heating pulse on the sensitive broadband detectors in the instrument has been eliminated. The well-behaved emission observed near the plasma edge, where lower optical depth enhances sensitivity to superthermals, as well as the good agreement between TVTS T_e profiles and ECE T_e profiles, indicates that only bulk electron heating is observed at higher densities ($N_e(0) > 1 \times 10^{13}$ cm^{-3}). In very low density discharges there is a clear indication that superthermal electrons are created during ECH.

The intense MHD activity induced in the plasma during on-axis ECH was somewhat surprising. This has not been previously observed[13,14] in other ECH experiments. As noted in Table I, the ECH antenna spot size was approximately 10 cm in diameter (10 dB points) at R = 140 cm. This is smaller than the diameter of the q = 1 region (~ 16 cm), as defined by the location of the inversion radius when sawteeth were present. Thus, for PDX, it is in fact reasonable that large amplitude sawteeth could be generated for on-axis heating. What is less comprehensible is that a displacement of the resonance zone of only 4 cm, which would mean that most of the ECH power is still deposited inside what should be the q = 1 surface, resulted in heating without any MHD activity.

Computer studies of these experiments using the same transport model for both on-axis and off-axis heating predicted the onset of sawtoothing for on-axis heating and the absence of sawtoothing for off-axis heating. Sawtooth behavior was a sensitive function of the plasma center - resonance zone separation for the χ_e model used in the simulation. Unfortunately, this limited set of data cannot be used to make more general statements about electron thermal conductivity. A more extensive study is needed and is planned to be done on PLT (Princeton Large Torus) in the near future.

The efficiency of electron cyclotron heating compares well with that observed with other heating methods. It is clear, however, that the intense MHD activity observed during on-axis heating must be taken into consideration in any calculation of heating efficiency. In contrast to these other heating methods, the MHD activity in the center of the discharge can be controlled simply by shifting the location of the resonance zone.

ACKNOWLEDGMENTS

We would like to thank N. Bowen, J. Doane, M. Goldman, P. Manintveld, R. Polman, M. Vocaturo, E. Fredd, N. Greenough, J. Lawson, and R. Sorenson for operating the ECH system; K. Bol, R. Fonck, R. Goldston, R. Kaita, S. Kaye, H. Kugel, K. McGuire, M. Okabayashi, G. Schmidt, and the PDX Group for their help and support during these experiments. Discussions with I. Fidone regarding the low density ECH experiments were most helpful.

The technical assistance of Robert Cutler on the grating polychromator is very much appreciated.

This work is supported by U.S. DOE Contract DE-AC02-76-CHO-3073.

REFERENCES

1 M. Bornatici et al., Nucl. Fusion 23, 1153 (1983).

2 Y. Carmel et al., Phys. Rev. Lett. 50, 112 (1983).

3 J.L. Doane, Princeton Plasma Physics Laboratory Report No. PPPL-2071, 1984.

4 H. Hsuan et al., Princeton Plasma Physics Laboratory Report No.PPPL-2114, 1984

5 J. Fischer, D. Boyd, A. Cavallo, J. Benson, Rev. Sci. Inst. 54, 1085 (1983).

6 QMC Instruments, Ltd., 229 Mile End Road, London, U.K.

7 L.J. Chu, J. App. Phys. 11, 603 (1940).

8 G. Tait, Fifth International Conference on IR and MM Waves, Wurzburg, W. Germany (October, 1980), paper T8-4.

9 D. Hwang et al., Phys. Rev. Lett. 51, 1865 (1983).

10 I. Fidone, G. Granata, R.L. Meyer, Plasma Phys. 22, 261, (1980).

11 TFR Group and I. Fidone, Phys. Rev. A, 24, 2861, 1981.

12 A. Silverman, D.E. Post, C.E. Singer, D.R. Mikkelsen, and the PPPL Transport Group, Princeton Plasma Physics Laboratory Report AP #23, 1983.

13 H. Piekaar, R.M. Sillen, Th. Oyevaar, A. Cavallo, I.R. 82/056, FOM Institute for Plasma Physics, Nieuwegein, the Netherlands, October, 1982.

14 R.M. Gilgenbach, A.E. England et al., Phys. Rev. Lett. 44, 647 (1980).

TABLE I

Summary of Experimental Conditions for the ECH Experiment

Plasma: $0.26 \times 10^{13}\ cm^{-3} < N_e(o) < 2.5 \times 10^{13}\ cm^{-3}$

$I_p = 250$ kA

$T_e(o) \approx 1.3$ keV

$P_{OH} \approx 250$ kW

$\bar{\tau}_{E_e} \approx 12$ msec

Electron-Electron Collision Time

$(N_e = 1.5 \times 10^{13}\ cm^{-3}\ T_e = 1.5\ keV) \approx 70\ \mu sec.$

Optical Depth - O-mode, 1st Harmonic

$(N_e = 10^{13}\ cm^{-3},\ T_e = 1.5\ keV,) \approx 1.56$ (80% single pass absorption)

RF System: 60 GHz - O-mode - Outside Antenna

Antenna Spot Size (R ≈ 140 cm) = 10 cm (10 dB points)

P_{RF} (gyrotron) = 100 kW

P_{RF} (into plasma) = 75 - 80 kW

TABLE II

BALDUR Transport Model for ECH Simulation

$$\chi_e = \chi_e \text{ (neoclassical)} + \frac{C_1}{N_e}\left[\frac{C_2 + \frac{r}{a}^{C_3}}{C_2 + (0.5)^{C_3}}\right]$$

Experimental PDX - ECH Data Fit with

$C_1 = 2 \times 10^{17}$ $\quad C_2 = 0.05$ $\quad C_3 = 1.0$

$\chi_i = 3\chi_i$ (Hinton-Haseltine neoclassical)

$D_H = D_H$ (neoclassical) $+ 2.7 \times 10^{16}/N_e$

Boundary Conditions:

$T_e(a) = T_i(a) = 40$ eV

$N_e(a) = 4 \times 10^{12}$ cm^{-3}

Here: N_e = electron density

$T_{e,i}$ = electron, ion temperature

r/a = normalized plasma radius

$\chi_{e,i}$ = electron/ion thermal conductivity

D_H = particle diffusivity

In addition:

Ohmic heating is determined using Spitzer Resistivity.

The model includes the Ware Pinch.

90% particle recycling is assumed.

FIGURE CAPTIONS

Fig. 1 Schematic of the 10 channel Grating Polychromator.

Fig. 2 The PDX light transport system.

Fig. 3 Electron temperature vs time at four radii for on-axis heating. The rapid rise of $T_e(r \approx -3$ cm) at the start of the ECH heating at 400 msec, the sawtooth activity in the central region of the plasma and the slow post-heating fall of T_e are seen most clearly in the insert. The full sawtooth amplitude is not shown here. The plasma/heating conditions for Figs. 3, 5, and 6 are $N_e(0) = 1.2 \times 10^{13}$ cm^{-3}, $I_p \simeq 260$ kA, $P_{RF} = 75$ kW, $R_{RES} = 135.5$ cm, $P_{OH} = 250$ kW, $t_E \simeq 12$ msec.

Fig. 4 MHD activity during on-axis ECH. From TVTS, full sawtooth amplitude is 900 eV, $\Delta T_e/T \approx 0.41$.

Fig. 5 TVTS-T_e profile compared with ECE T_e profile at the top of an ECH sawtooth. Note that the grating instrument was not set to observe the peak temperature of the sawooth.

Fig. 6 Comparison of TVTS and ECE T_e profiles at 700 μ sec after sawtooth collapse.

Fig. 7 Electron temperature vs time for off-axis ECH. The rapid initial rise, the lack of MHD activity and the unexpectedly slow fall of the central T_e can be seen in the insert. The plasma/heating parameters for the discharges shown in Figs. 7 and 8 are: $I_p \approx 250$ kA, $N_e(0) \approx 2.1 \times 10^{13}$ cm^{-3}, $P_{RF} = 80$ kW, $R_{RES} = 141.7$ cm, $R_o \approx 136$ cm.

Fig. 8 Off-axis heating; a comparison of TVTS and ECE profiles at 440 msec (the end of the 40 msec heating pulse).

Fig. 9 Line averaged density, plasma current (I_p), and loop voltage for a typical ECH experiment.

Fig. 10 ECH heating of a low density plasma: I_p = 250 kA, P_{RF} = 70 kW, R_{RES} = 135 cm, $\bar{N}_e$ = 0.13 x 10^{13} cm^{-3}.

Fig. 11 A. T_e profile before ECH, BALDUR simulation TVTS, and ECE data compared, t = 400 ms.

B. T_e profile after ECH, resonance zone 4 cm off-axis. BALDUR simulation, TVTS and ECE data compared t = 440 ms.

Fig. 12 A. Computer simulation of $T_e(0)$ vs time. $\bar{N}_e$ evolution shown in insert.

B. Experimental data $T_e(0)$ vs time. $\bar{N}_e$ programmed to return to its preheating value (insert).

#83X0898

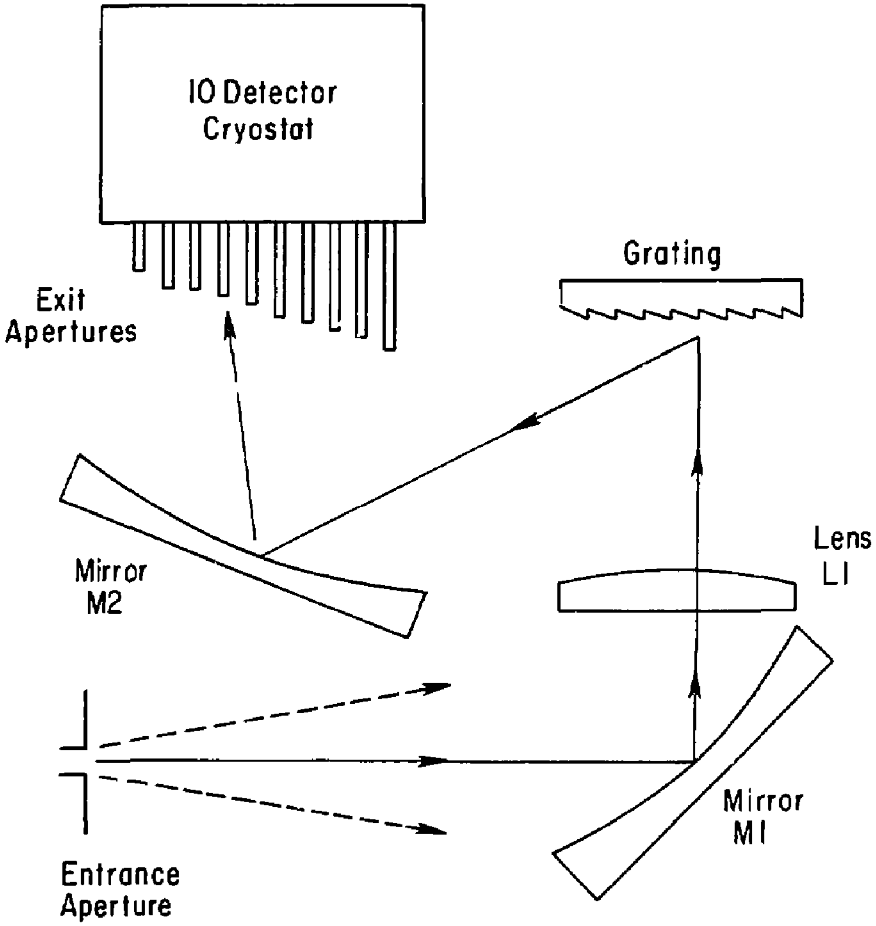

10 CHANNEL GRATING POLYCHROMATOR

Fig. 1

#83X0899

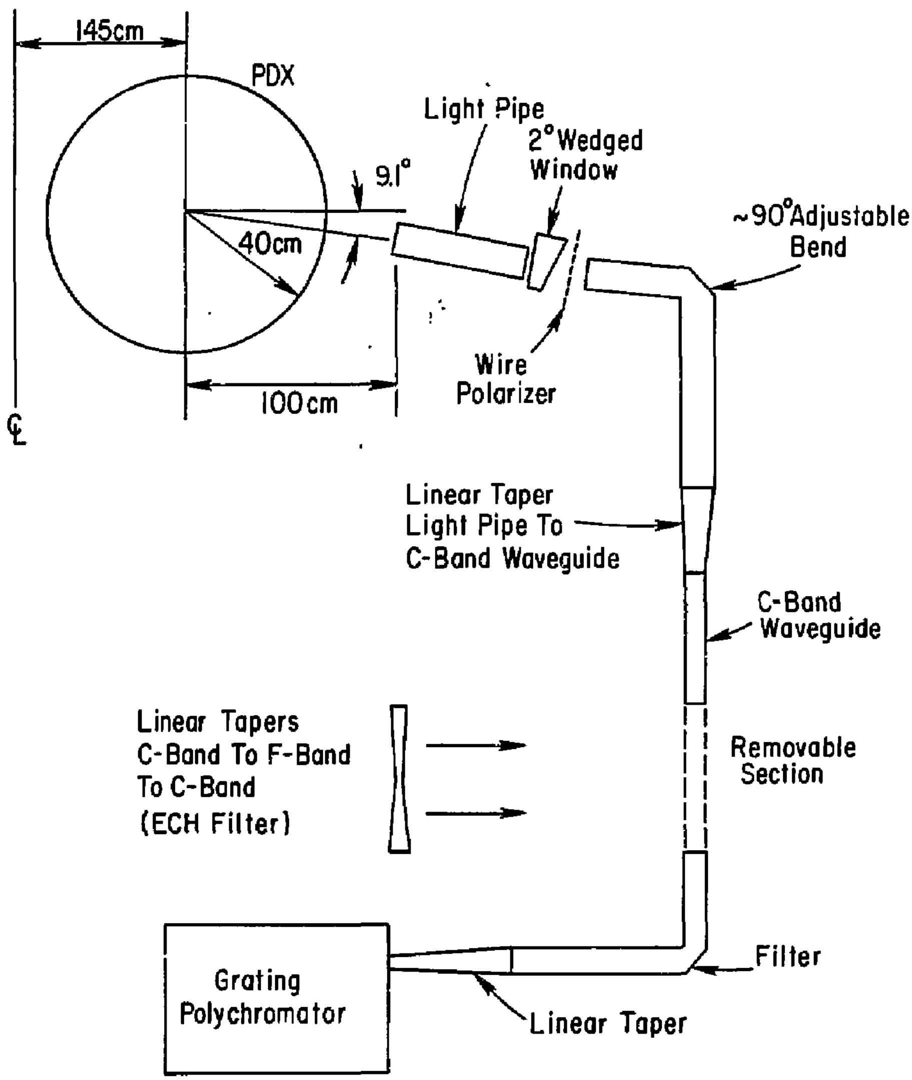

Fig. 2

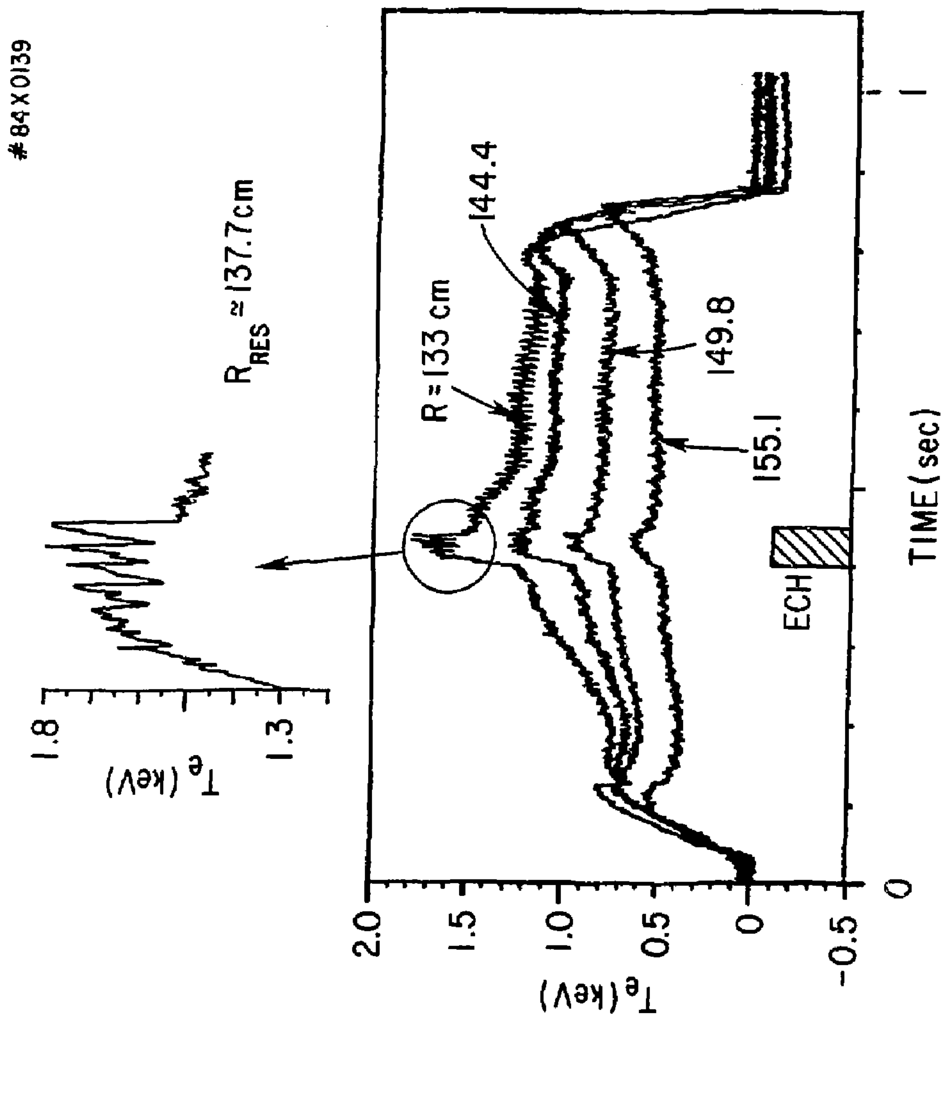

#84X0139
$R_{RES} \simeq 137.7$ cm
T_e (keV)
1.8
1.3
R = 133 cm
144.4
149.8
155.1
ECH
TIME (sec)
T_e (keV)
2.0
1.5
1.0
0.5
0
−0.5
0
1

Fig. 3

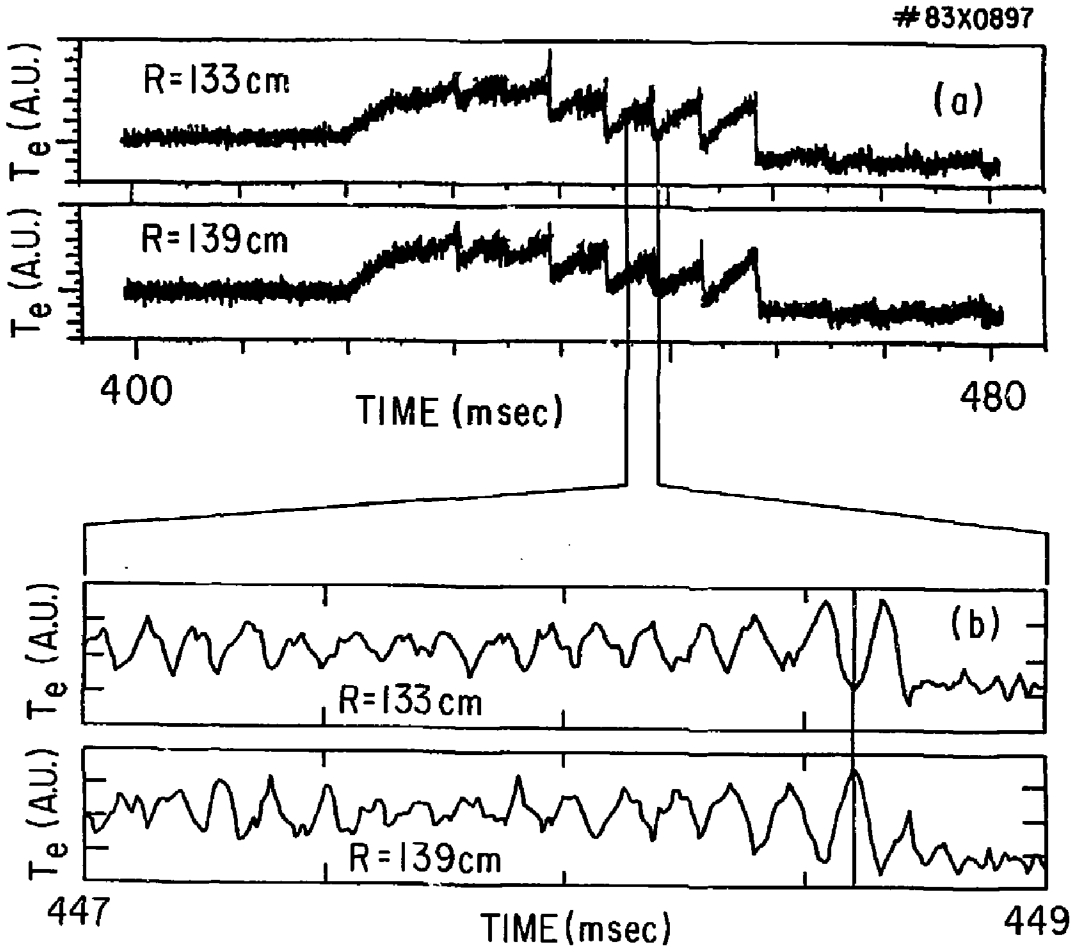

#83X0897
(a)
R=133cm
R=139cm
T_e (A.U.)
T_e (A.U.)
400
480
TIME (msec)
(b)
R=133cm
R=139cm
T_e (A.U.)
T_e (A.U.)
447
449
TIME (msec)

Fig. 4

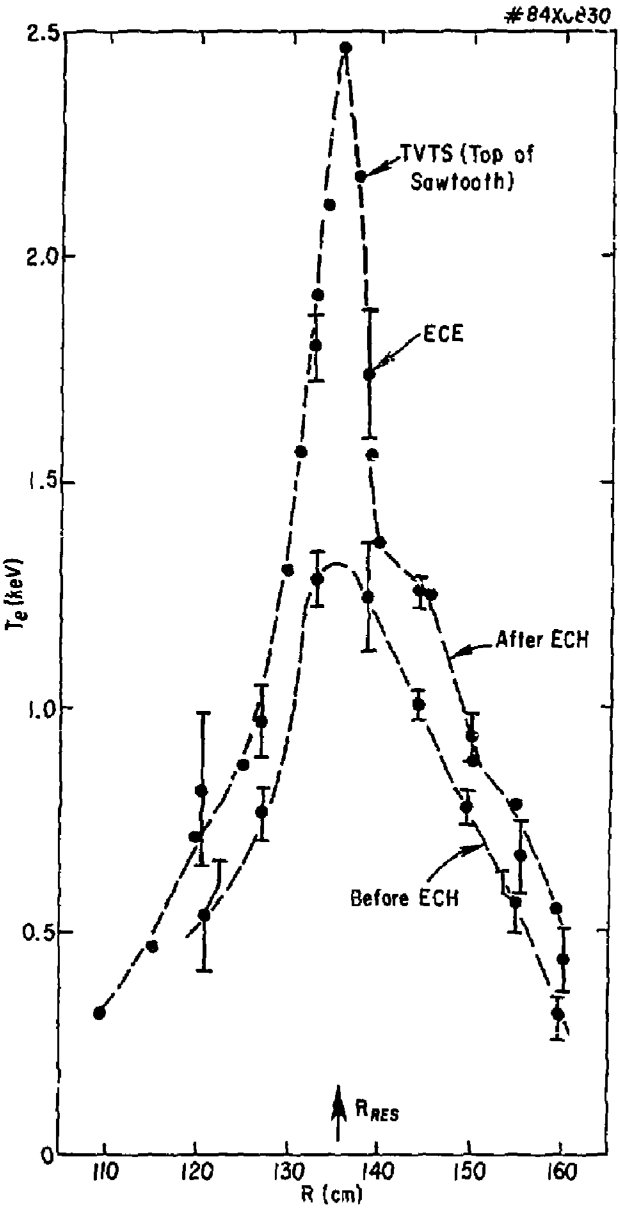
#84X0830
2.5
2.0
1.5
1.0
0.5
0
Te (keV)
TVTS (Top of Sawtooth)
ECE
After ECH
Before ECH
RRES
110
120
130
140
150
160
R (cm)

Fig. 5

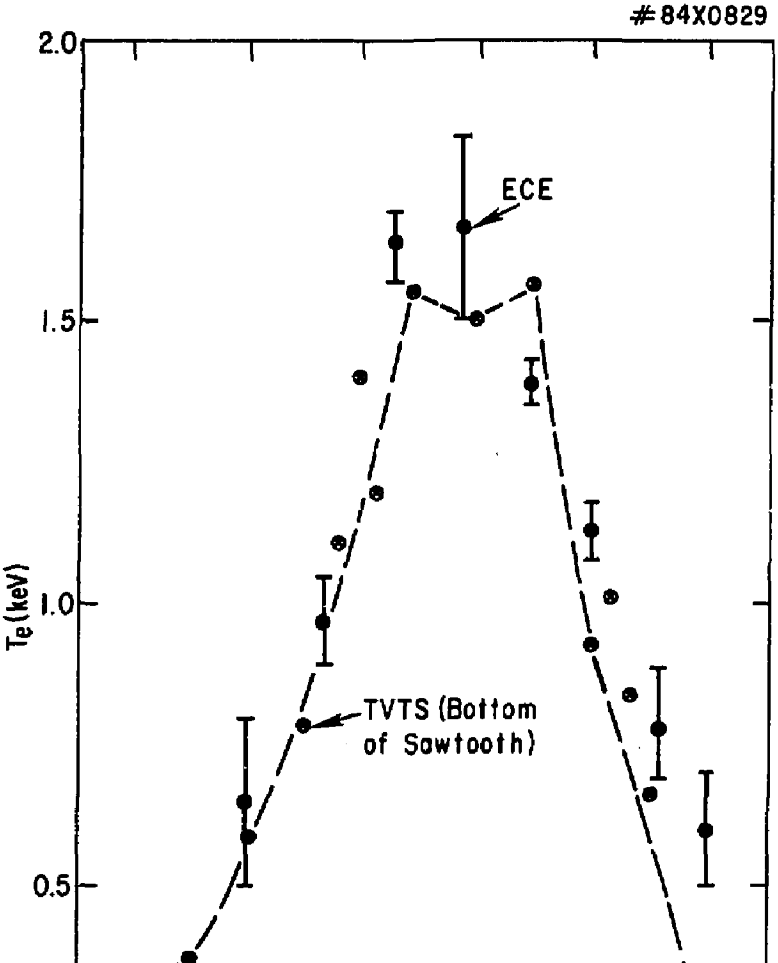

#84X0829
2.0
1.5
1.0
0.5
0
T_e (keV)
ECE
TVTS (Bottom of Sawtooth)
R_{RES}
110
120
130
140
150
160
R (cm)

Fig. 6

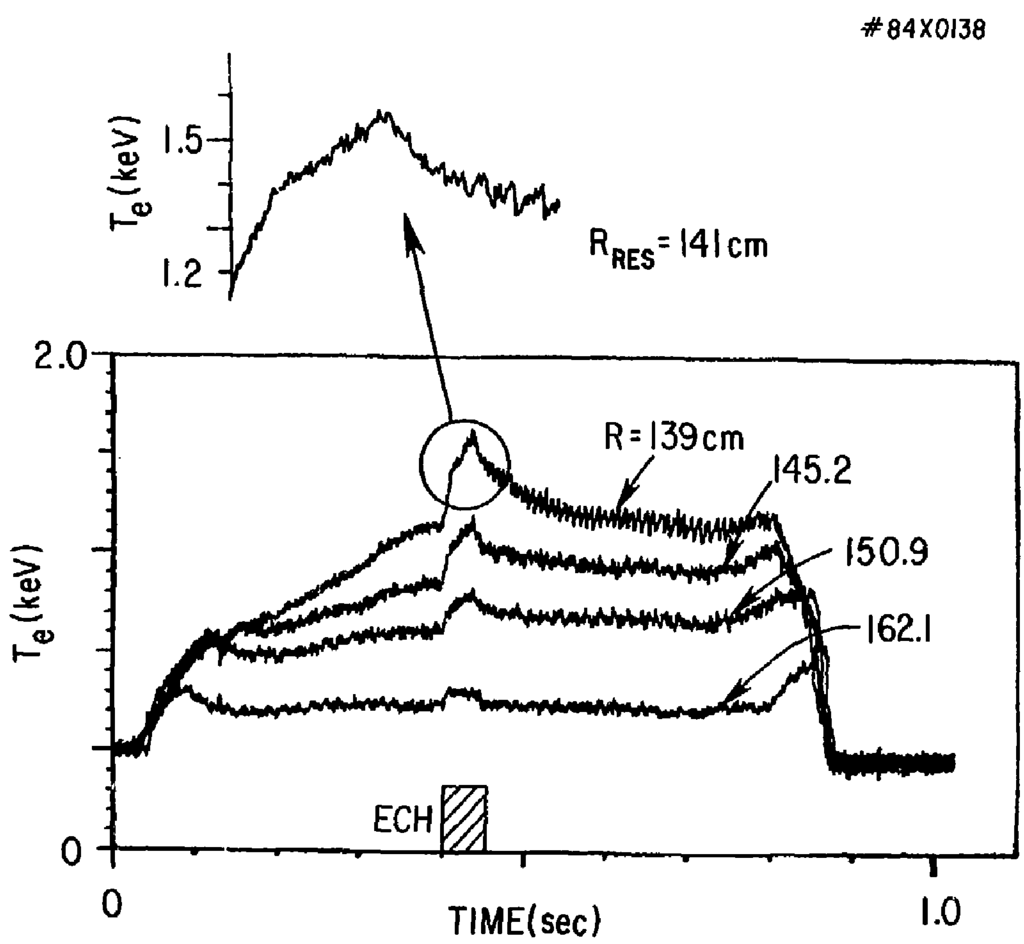

#84X0138
T_e (keV)
1.5
1.2
R_{RES} = 141 cm
2.0
0
R = 139 cm
145.2
150.9
162.1
ECH
0
TIME(sec)
1.0

Fig. 7

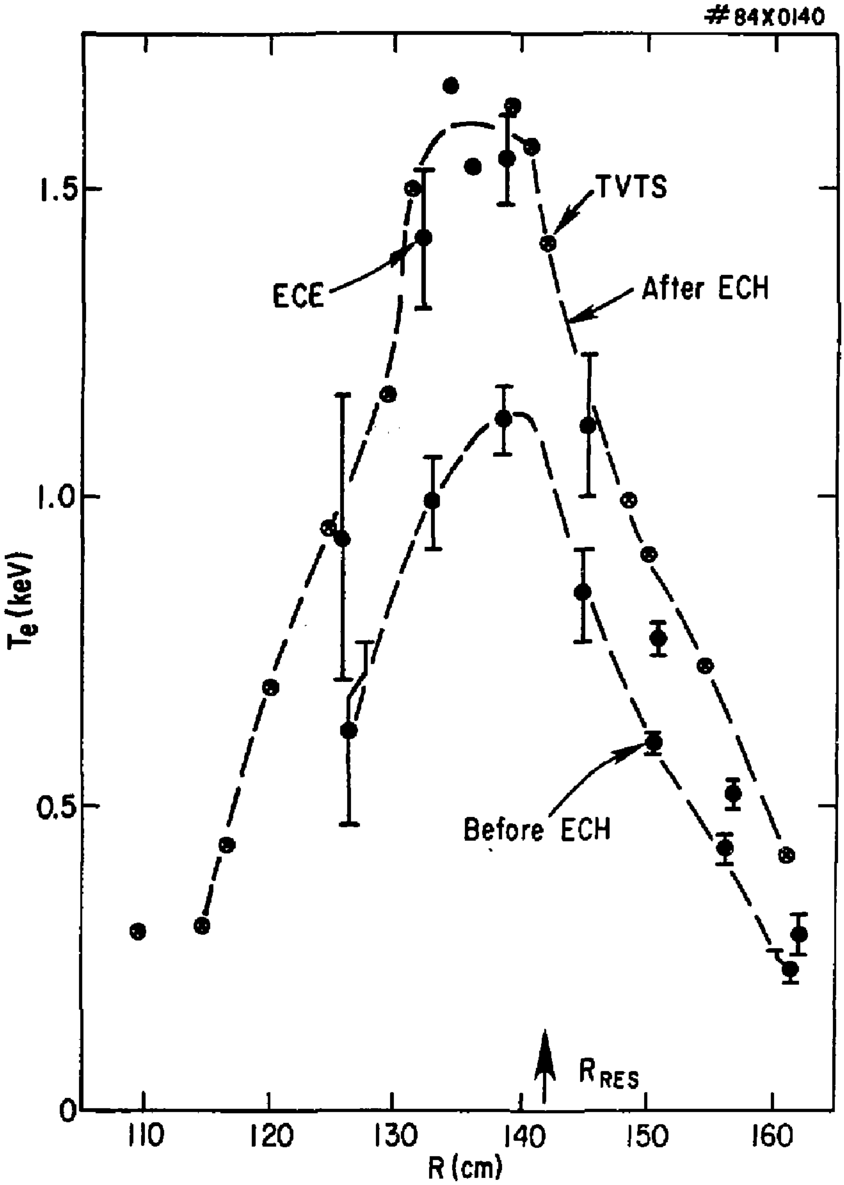

#84X0140
1.5
1.0
0.5
0
Te (keV)
TVTS
ECE
After ECH
Before ECH
RRES
110
120
130
140
150
160
R (cm)

Fig. 8

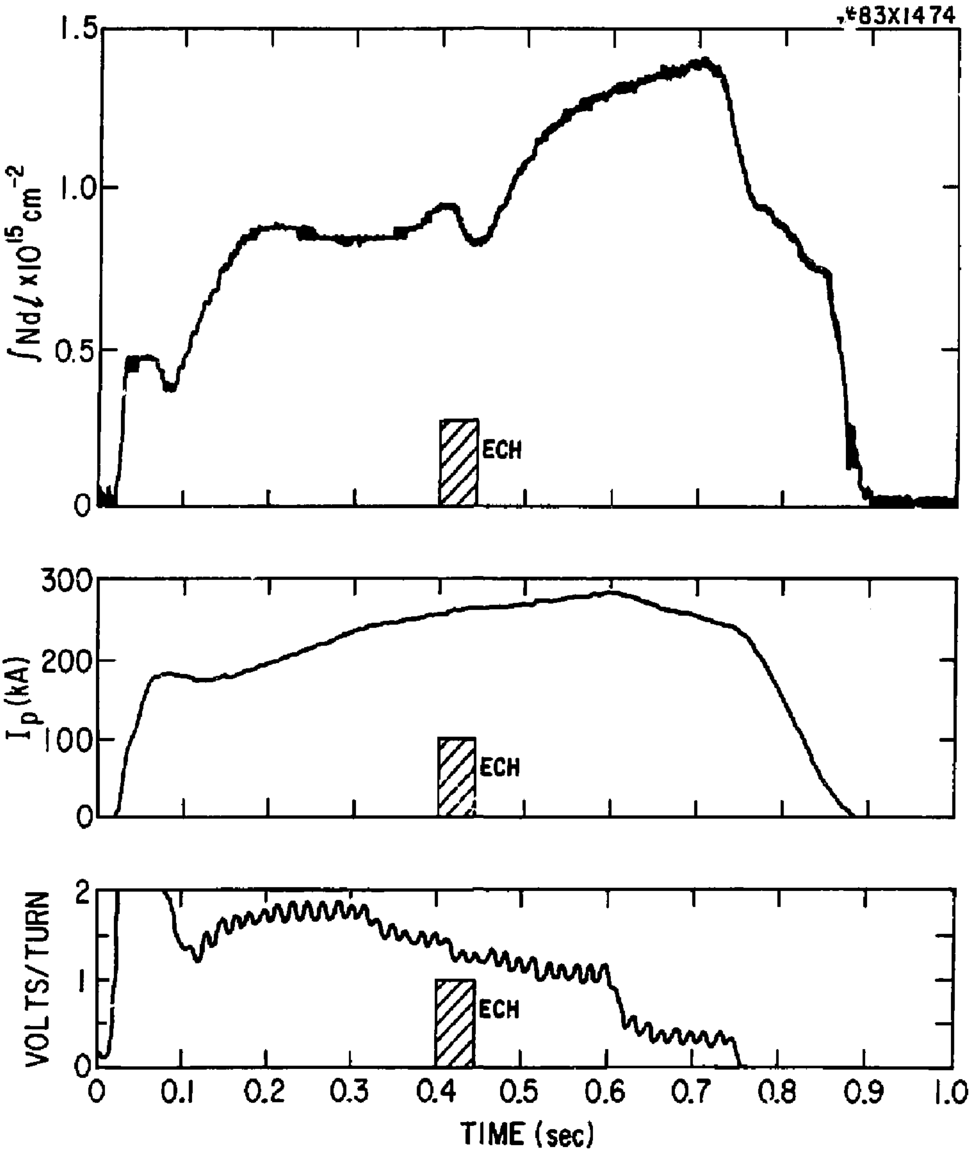
#83X1474
1.5
1.0
0.5
0
∫Ndℓ / x10^15 cm^-2
ECH
300
200
100
0
Ip (kA)
ECH
2
1
0
VOLTS/TURN
ECH
0
0.1
0.2
0.3
0.4
0.5
0.6
0.7
0.8
0.9
1.0
TIME (sec)

Fig. 9

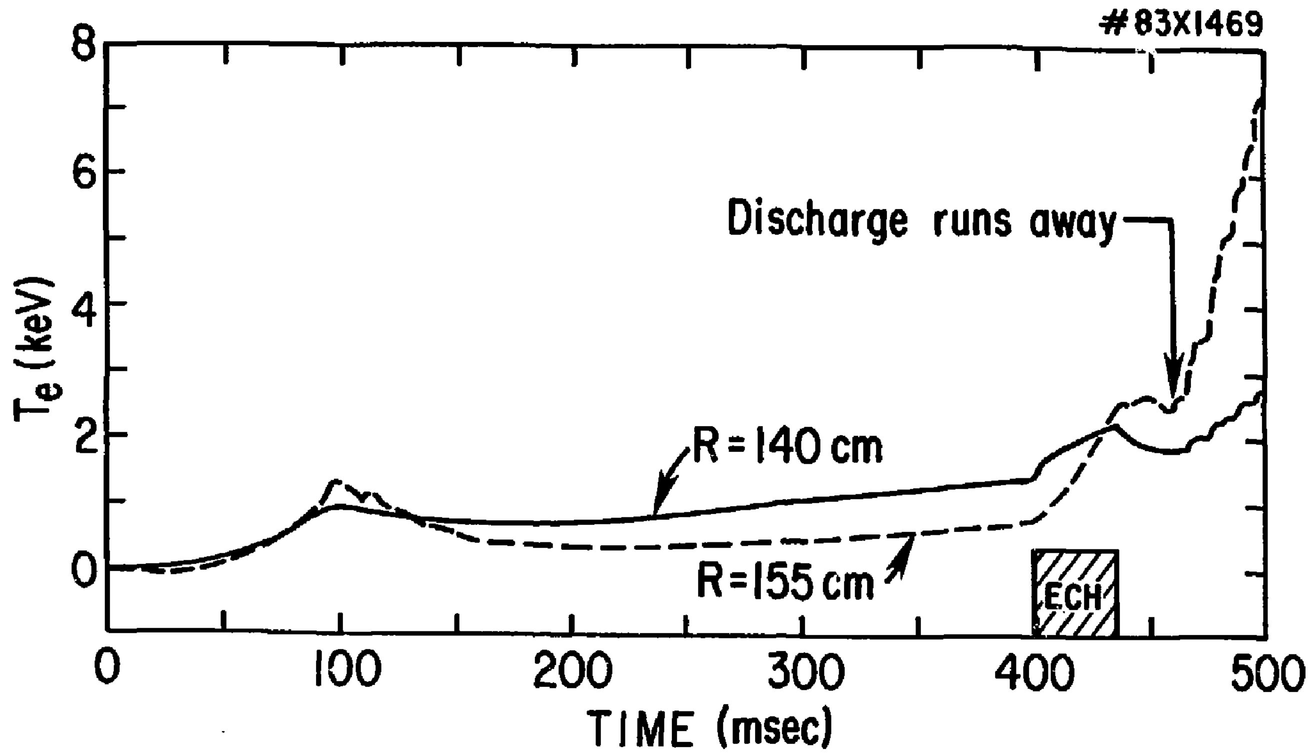
#83X1469
Discharge runs away
R=140 cm
R=155 cm
ECH
T_e (keV)
TIME (msec)
0
100
200
300
400
500
0
2
4
6
8

Fig. 10

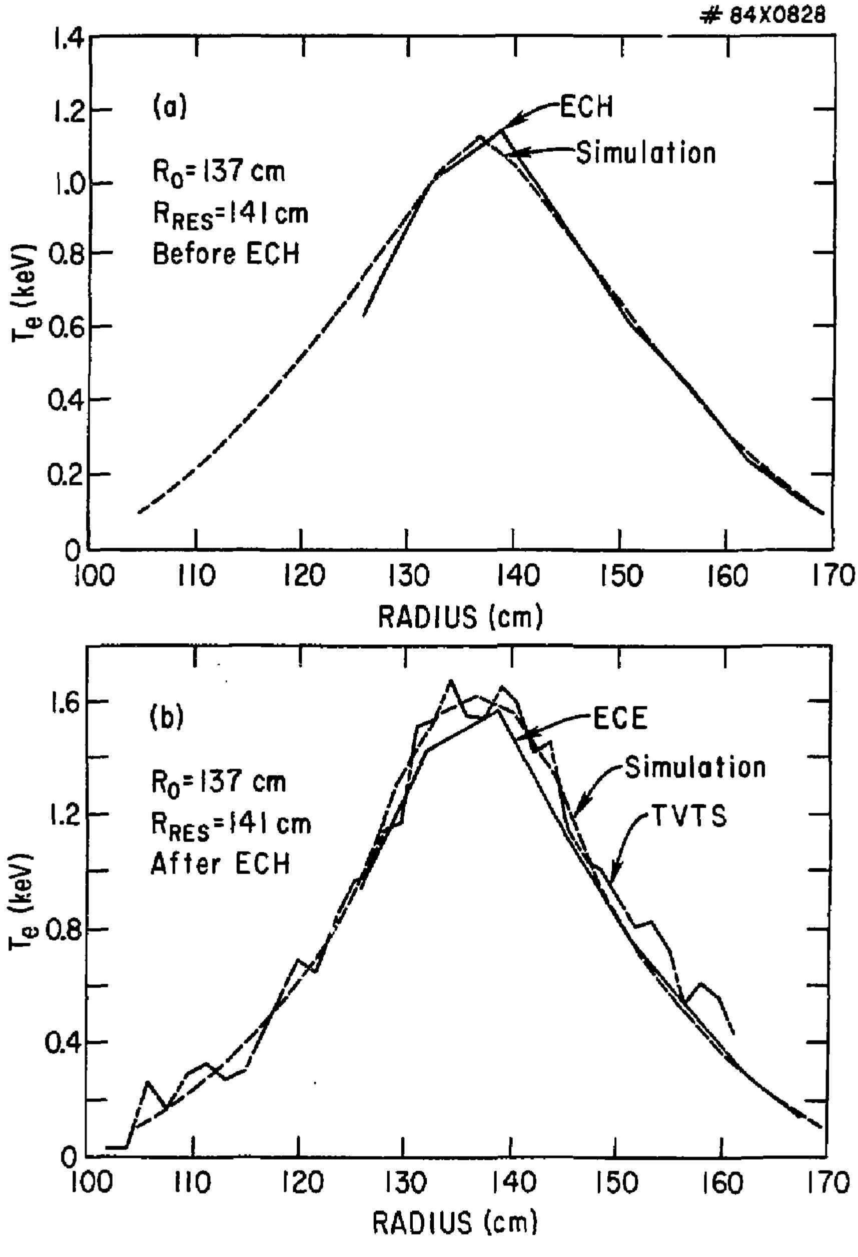

84X0828
(a)
R0=137 cm
RRES=141 cm
Before ECH
ECH
Simulation
Te (keV)
RADIUS (cm)
(b)
R0=137 cm
RRES=141 cm
After ECH
ECE
Simulation
TVTS
Te (keV)
RADIUS (cm)

Fig. 11

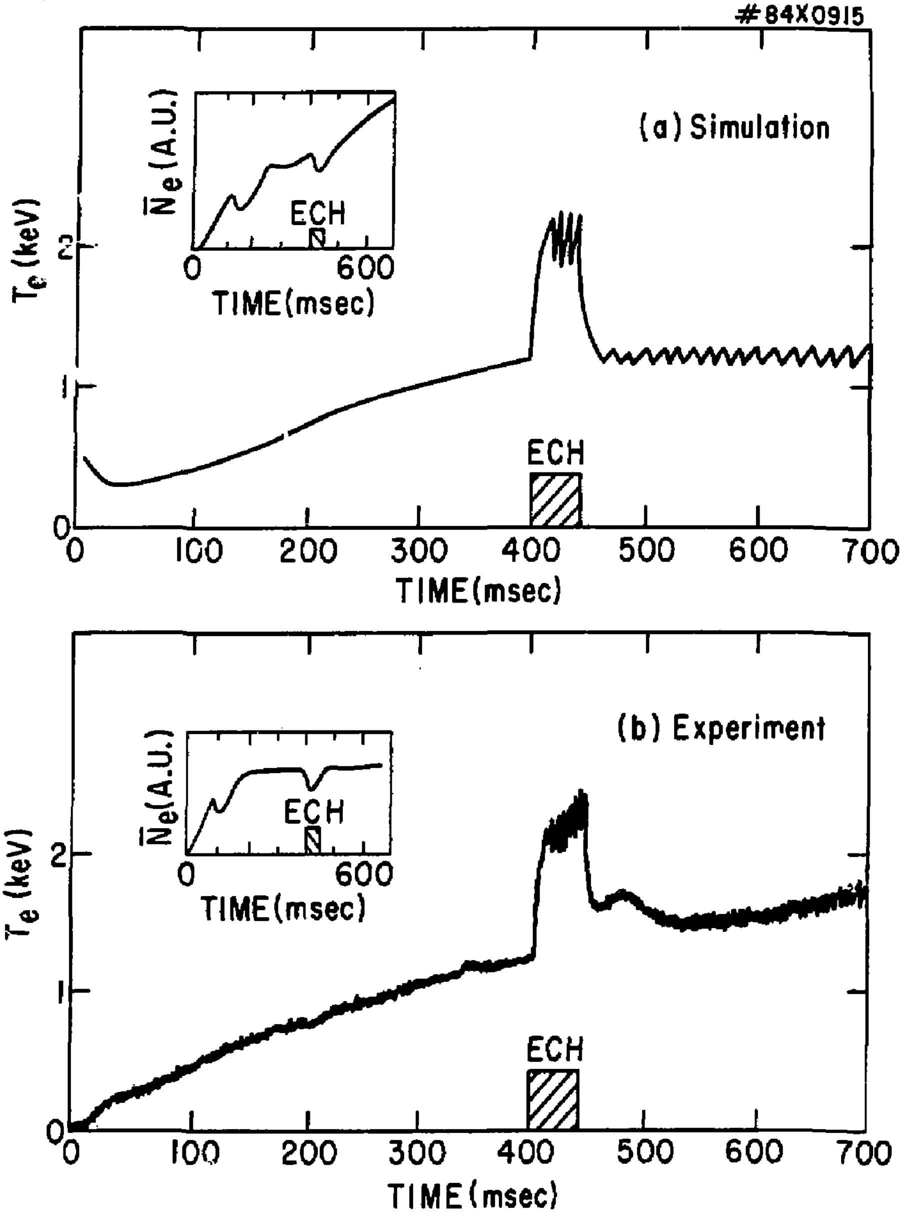
#84X0915
(a) Simulation
$\bar{N}_e$ (A.U.)
ECH
0
600
TIME(msec)
T_e (keV)
0
1
2
ECH
0
100
200
300
400
500
600
700
TIME(msec)
(b) Experiment
$\bar{N}_e$(A.U.)
ECH
0
600
TIME(msec)
T_e (keV)
0
1
2
ECH
0
100
200
300
400
500
600
700
TIME(msec)

Fig. 12

EXTERNAL DISTRIBUTION IN ADDITION TO TIC UC-20

Plasma Res Lab, Austra Nat'l Univ, AUSTRALIA
Dr. Frank J. Paoloni, Univ of Wollongong, AUSTRALIA
Prof. I.R. Jones, Flinders Univ., AUSTRALIA
Prof. M.H. Brennan, Univ Sydney, AUSTRALIA
Prof. F. Cap, Inst Theo Phys, AUSTRIA
Prof. Frank Verheest, Inst theoretische, BELGIUM
Dr. D. Palumbo, Dg XII Fusion Prog, BELGIUM
Ecole Royale Militaire, Lab de Phys Plasmas, BELGIUM
Dr. P.H. Sakanaka, Univ Estadual, BRAZIL
Dr. C.R. James, Univ of Alberta, CANADA
Prof. J. Teichmann, Univ of Montreal, CANADA
Dr. H.M. Skarsgard, Univ of Saskatchewan, CANADA
Prof. S.R. Sreenivasan, University of Calgary, CANADA
Prof. Tudor W. Johnston, INRS-Energie, CANADA
Dr. Hannes Barnard, Univ British Columbia, CANADA
Dr. M.P. Bachynski, MPB Technologies, Inc., CANADA
Zhengwu Li, SW Inst Physics, CHINA
Library, Tsing Hua University, CHINA
Librarian, Institute of Physics, CHINA
Inst Plasma Phys, Academia Sinica, CHINA
Dr. Peter Lukac, Komenskeho Univ, CZECHOSLOVAKIA
The Librarian, Culham Laboratory, ENGLAND
Prof. Schatzman, Observatoire de Nice, FRANCE
J. Radet, CEN-BP6, FRANCE
AM Dupas Library, AM Dupas Library, FRANCE
Dr. Tom Mual, Academy Bibliographic, HONG KONG
Preprint Library, Cent Res Inst Phys, HUNGARY
Dr. S.K. Trehan, Panjab University, INDIA
Dr. Indra, Mohan Lal Das, Banaras Hindu Univ, INDIA
Dr. L.K. Chavda, South Gujarat Univ, INDIA
Dr. R.K. Chhajlani, Var Ruchi Marg, INDIA
P. Kaw, Physical Research Lab, INDIA
Dr. Phillip Rosenau, Israel Inst Tech, ISRAEL
Prof. S. Cuperman, Tel Aviv University, ISRAEL
Prof. G. Rostagni, Univ Di Padova, ITALY
Librarian, Int'l Ctr Theo Phys, ITALY
Miss Clelia De Palo, Assoc EURATOM-CNEN, ITALY
Biblioteca, del CNR EURATOM, ITALY
Dr. H. Yamato, Toshiba Res & Dev, JAPAN
Prof. M. Yoshikawa, JAERI, Tokai Res Est, JAPAN
Prof. T. Uchida, University of Tokyo, JAPAN
Research Info Center, Nagoya University, JAPAN
Prof. Kyoji Nishikawa, Univ of Hiroshima, JAPAN
Prof. Sigeru Mori, JAERI, JAPAN
Library, Kyoto University, JAPAN
Prof. Ichiro Kawakami, Nihon Univ, JAPAN
Prof. Satoshi Itoh, Kyushu University, JAPAN
Tech Info Division, Korea Atomic Energy, KOREA
Dr. R. England, Civdad Universitaria, MEXICO
Bibliotheek, Fom-Inst Voor Plasma, NETHERLANDS
Prof. B.S. Liley, University of Waikato, NEW ZEALAND
Dr. Suresh C. Sharma, Univ of Calabar, NIGERIA
Prof. J.A.C. Cabral, Inst Superior Tech, PORTUGAL
Dr. Octavian Petrus, ALI CUZA University, ROMANIA
Prof. M.A. Hellberg, University of Natal, SO AFRICA
Dr. Johan de Villiers, Atomic Energy Bd, SO AFRICA
Fusion Div. Library, JEN, SPAIN
Prof. Hans Wilhelmson, Chalmers Univ Tech, SWEDEN
Dr. Lennart Stenflo, University of UMEA, SWEDEN
Library, Royal Inst Tech, SWEDEN
Dr. Erik T. Karlson, Uppsala Universitet, SWEDEN
Centre de Recherchesen, Ecole Polytech Fed, SWITZERLAND
Dr. W.L. Weise, Nat'l Bur Stand, USA
Dr. W.M. Stacey, Georg Inst Tech, USA
Dr. S.T. Wu, Univ Alabama, USA
Prof. Norman L. Oleson, Univ S Florida, USA
Dr. Benjamin Ma, Iowa State Univ, USA
Prof. Magne Kristiansen, Texas Tech Univ, USA
Dr. Raymond Askew, Auburn Univ, USA
Dr. V.T. Tolok, Kharkov Phys Tech Ins, USSR
Dr. D.D. Ryutov, Siberian Acad Sci, USSR
Dr. G.A. Eliseev, Kurchatov Institute, USSR
Dr. V.A. Glukhikh, Inst Electro-Physical, USSR
Institute Gen. Physics, USSR
Prof. T.J. Boyd, Univ College N Wales, WALES
Dr. K. Schindler, Ruhr Universitat, W. GERMANY
Nuclear Res Estab, Julich Ltd, W. GERMANY
Librarian, Max-Planck Institut, W. GERMANY
Dr. H.J. Kaeppler, University Stuttgart, W. GERMANY
Bibliothek, Inst Plasmaforschung, W. GERMANY